Title

18F-FDG Dedicated Breast PET Complementary to Breast MRI for Evaluating Early Response to Neoadjuvant Chemotherapy.

Journal

Radiology: Imaging Cancer, 6(2)

Authors

Diwanji, Devan
Onishi, Natsuko
Hathi, Deep
et al.

Publication Date

2024-03-01

DOI

10.1148/rycan.230082

Peer reviewed

Radiology: Imaging Cancer

ORIGINAL RESEARCH

^{18}F-FDG Dedicated Breast PET Complementary to Breast MRI for Evaluating Early Response to Neoadjuvant Chemotherapy

Devan Diwanji, MD, PhD • Natsuko Onishi, MD, PhD • Deep K. Hathi, PhD • Courtney Lawhn-Heath, MD • John Kornak, PhD • Wen Li, PhD • Ruby Guo, AB • Julissa Molina-Vega, BA • Youngho Seo, PhD • Robert R. Flavell, MD, PhD • Diane Heditsian, BA • Susie Brain, BSc • Laura J. Esserman, MD, MBA • Bonnie N. Joe, MD, PhD • Nola M. Hylton, PhD • Ella F. Jones, PhD • Kimberly M. Ray, MD

From the Departments of Radiology and Biomedical Imaging (D.D., N.O., D.K.H., C.L.H., W.L., R.G., Y.S., R.R.F., B.N.J., N.M.H., E.F.J., K.M.R.), Epidemiology and Biostatistics (J.K.), and Surgery (J.M.V., L.J.E.), University of California San Francisco, 550 16th St, San Francisco, CA 94158; and I-SPY 2 Advocacy Group, San Francisco, Calif (D.H., S.B.). Received August 8, 2023; revision requested September 13; final revision received December 30; accepted February 16, 2024. **Address correspondence to** K.M.R. (email: *kimberly.ray@ucsf.edu*).

Supported by the National Institutes of Health (grants 1F30 CA247147, U01 CA225427, R01 CA227763, P01 CA210961, P01 CA123916, and R01 CA132870) and U.S. Department of Defense (grant W81XWH-18-1-0671). The I-SPY 2 TRIAL is supported by Quantum Leap Healthcare Collaborative (2013 to present).

Conflicts of interest are listed at the end of this article.

Radiology: Imaging Cancer 2024; 6(2):e230082 • https://doi.org/10.1148/rycan.230082 • Content codes: BR MR

Purpose: To compare quantitative measures of tumor metabolism and perfusion using fluorine 18 (^{18}F) fluorodeoxyglucose (FDG) dedicated breast PET (dbPET) and breast dynamic contrast-enhanced (DCE) MRI during early treatment with neoadjuvant chemotherapy (NAC).

Materials and Methods: Prospectively collected DCE MRI and ^{18}F-FDG dbPET examinations were analyzed at baseline (T0) and after 3 weeks (T1) of NAC in 20 participants with 22 invasive breast cancers. FDG dbPET–derived standardized uptake value (SUV), metabolic tumor volume, and total lesion glycolysis (TLG) and MRI-derived percent enhancement (PE), signal enhancement ratio (SER), and functional tumor volume (FTV) were calculated at both time points. Differences between FDG dbPET and MRI parameters were evaluated after stratifying by receptor status, Ki-67 index, and residual cancer burden. Parameters were compared using Wilcoxon signed rank and Mann-Whitney *U* tests.

Results: High Ki-67 tumors had higher baseline SUV_{mean} (difference, 5.1; $P = .01$) and SUV_{peak} (difference, 5.5; $P = .04$). At T1, decreases were observed in FDG dbPET measures (pseudo-median difference T0 minus T1 value [95% CI]) of SUV_{max} (−6.2 [−10.2, −2.6]; $P < .001$), SUV_{mean} (−2.6 [−4.9, −1.3]; $P < .001$), SUV_{peak} (−4.2 [−6.9, −2.3]; $P < .001$), and TLG (−29.1 mL^3 [−71.4, −6.8]; $P = .005$) and MRI measures of SER_{peak} (−1.0 [−1.3, −0.2]; $P = .02$) and FTV (−11.6 mL^3 [−22.2, −1.7]; $P = .009$). Relative to nonresponsive tumors, responsive tumors showed a difference (95% CI) in percent change in SUV_{max} of −34.3% (−55.9%, 1.5%; $P = .06$) and in PE_{peak} of −42.4% (95% CI: −110.5%, 8.5%; $P = .08$).

Conclusion: ^{18}F-FDG dbPET was sensitive to early changes during NAC and provided complementary information to DCE MRI that may be useful for treatment response evaluation.

Clinical trial registration no. NCT01042379

Supplemental material is available for this article.

Breast cancer is a heterogeneous disease requiring therapies specifically targeted to an individual patient's tumor characteristics (1–5). Treatment decisions can be further refined based on gene expression assays that probe an array of molecular markers for an individual tumor (3). For more aggressive and advanced breast cancers, neoadjuvant chemotherapy (NAC) permits the study of the individual patient's response to targeted therapy (6–8). The response of the primary breast tumor to NAC is a surrogate marker for the response of systemic micrometastases and predicts long-term survival outcomes (9,10). Thus, there is a critical need to develop predictive biomarkers that can help assess response to NAC. Furthermore, effective evaluation of treatment response is required early in the course of NAC, both to triage patients toward the most effective regimen and to avoid the toxicity of ineffective treatments.

Imaging provides a noninvasive means of assessing treatment response and predicting pathologic complete response and residual cancer burden (RCB). MRI-derived measures of peak signal enhancement ratio (SER) and functional tumor volume (FTV) have been shown to be superior to clinicopathologic examination in predicting response to NAC and survival outcomes (11,12). Fluorine 18 fluorodeoxyglucose (FDG) PET is a powerful functional imaging technique that captures tumor glycolysis and has the potential to detect early response to therapy before morphologic changes are visible on anatomic images. Numerous studies have demonstrated the utility of whole-body PET (wbPET) with FDG in monitoring the

Abbreviations

dbPET = dedicated breast PET, DCE = dynamic contrast-enhanced, FDG = fluorodeoxyglucose, FTV = functional tumor volume, HER2 = human epidermal growth factor receptor 2, HR = hormone receptor, MTV = metabolic tumor volume, NAC = neoadjuvant chemotherapy, PE = percent enhancement, RCB = residual cancer burden, SER = signal enhancement ratio, SUV = standardized uptake value, TLG = total lesion glycolysis, TNBC = triple-negative breast cancer, wbPET = whole-body PET

Summary

Results of this exploratory study suggest that fluorine 18 fluorodeoxyglucose dedicated breast PET provides nonredundant information relative to breast MRI and is highly sensitive to metabolic changes early in the course of neoadjuvant chemotherapy.

Key Points

- After 3 weeks of neoadjuvant chemotherapy (NAC), primary breast tumors demonstrated decreases in fluorodeoxyglucose dedicated breast PET measures (pseudo-median difference T0 minus T1 value [95% CI]) of maximum standardized uptake value (SUV) (−6.2 [−10.2, −2.6]; $P < .001$), SUV_{mean} (−2.6 [−4.9, −1.3]; $P < .001$), SUV_{peak} (−4.2 [−6.9, −2.3]; $P < .001$), and total lesion glycolysis (−29.1 mL^3 [−71.4, −6.8]; $P = .005$).
- Decreases in dynamic contrast-enhanced breast MRI measures (pseudo-median difference T0 minus T1 value [95% CI]) of peak signal enhancement ratio (−1.0 [−1.3, −0.2]; $P = .02$) and functional tumor volume (−11.6 mL^3 [−22.2, −1.7]; $P = .009$) were observed in primary breast tumors after 3 weeks of NAC.
- Relative to nonresponsive tumors, treatment-responsive tumors showed a difference (95% CI) in percent changes in SUV_{max} of −34.3% (−55.9%, 1.5%; $P = .06$) and in peak percent enhancement of −42.4% (−110.5%, 8.5%; $P = .08$) after 3 weeks of NAC.

Keywords

Breast, PET, Dynamic Contrast-enhanced MRI

response of breast cancer to NAC at earlier time points than MRI (13–15). Standardized uptake values (SUVs) from wbPET have been correlated with angiogenic biomarkers (16), tumor vascularity (17), molecular subtypes (18,19), MRI kinetics (19), and response to treatment (20–22).

Despite its predictive value, wbPET is limited in characterizing primary breast tumors, and dedicated breast PET (dbPET) scanners have been developed to address wbPET limitations and to permit more detailed functional characterization of primary breast tumors. While prone positioning is feasible with wbPET, supine patient positioning is most commonly used; the latter collapses breast tissue and contributes to respiratory motion blurring (23). Partial volume effects also limit the spatial resolution of wbPET (24). The dbPET scanner consists of a ring of detectors that translates axially over the length of the breast (25). Patients undergo imaging in the prone position without breast compression. dbPET has higher spatial resolution (1–2 mm) compared with wbPET (4–6 mm), and previous studies have shown it has increased sensitivity for primary tumor detection, particularly for lesions measuring less than 1 cm (26). dbPET has also been shown to have a greater dynamic range compared with wbPET, which may enable more sensitive measurement and stratification of treatment response. Because of its high sensitivity, dbPET requires half the dose of FDG relative to wbPET, a desirable feature when repeated longitudinal assessments of primary breast tumors during NAC are needed. Owing to its high spatial resolution, dbPET has been shown to be superior to wbPET in depicting intratumoral heterogeneity (27,28), a potentially important predictive and prognostic marker (1,4). Finally, in the clinical trial setting, receptor-specific tracers can be used to probe different breast cancer subtypes to permit more detailed assessment of response to targeted therapies.

Although dbPET is a Food and Drug Administration–approved device, it is currently applied only in the experimental setting in the United States, and its role in characterizing and monitoring primary breast cancers is not well established. There are limited data on the sensitivity and accuracy of dbPET in assessing early response to NAC, the comparative performance of dbPET and MRI assessment during early treatment, and the relationship between dbPET parameters and immunohistochemical markers. In this pilot study, which represents early-stage work, we imaged biopsy-confirmed primary invasive breast cancers with both MRI and FDG dbPET at baseline and 3 weeks after NAC initiation. Quantitative FDG dbPET and MRI parameters were measured and compared. In addition, we performed exploratory analyses to study the relationship between these imaging parameters and immunohistochemical markers as well as RCB status upon treatment completion. Last, the correlation between FDG dbPET and MRI parameters was assessed to better understand the relationships between tumor metabolism and tumor vascularity.

Materials and Methods

This study followed a Health Insurance Portability and Accountability Act–compliant study protocol that was reviewed by the institutional review board of University of California San Francisco, and approved by the Committee of Human Research of the University of California San Francisco, under the institution's Human Research Protection Program. All study participants provided written informed consent.

Study Participants

This study prospectively coenrolled individuals participating in the I-SPY 2 TRIAL (Investigation of Serial Studies to Predict Your Therapeutic Response with Imaging and Molecular Analysis 2; ClinicalTrials.gov: NCT01042379) between November 2015 and November 2021 who underwent FDG dbPET imaging at time points corresponding to their breast dynamic contrast-enhanced (DCE) MRI examinations at baseline (T0) and at 3-week follow-up of NAC (T1). The I-SPY 2 TRIAL is an ongoing multicenter adaptively randomized phase 2 trial with multiple neoadjuvant therapy arms for individuals with breast cancer at high risk for early recurrence. During the screening process for enrollment in the I-SPY 2 TRIAL at the University of California San Francisco, 20 participants diagnosed with biopsy-proven invasive breast carcinoma were coenrolled in this study, which included additional FDG dbPET imaging. All participants coenrolled in this study underwent DCE MRI and FDG dbPET at baseline (T0); 17 participants also completed 3-week follow-up of NAC (T1) with dbPET, and 15 completed follow-up MRI.

Female individuals aged 18 years or older diagnosed with stage II or III breast cancer (tumor size > 2.5 cm) without distant metastases were eligible for the screening process of the I-SPY 2 TRIAL. Individuals with hormone receptor (HR)–positive/human epidermal growth factor receptor 2 (HER2)–negative tumors that were assessed as low risk using a 70-gene assay (MammaPrint; Agendia) were screened out of the trial. I-SPY 2 TRIAL participants were administered 12 cycles of weekly paclitaxel (standard of care) and/or a combination of experimental agents for 12 weeks, followed by four cycles of anthracycline-cyclophosphamide before the surgical procedure to remove the primary tumor. Participants with HER2+ cancer were also administered trastuzumab for the first 12 weeks.

FDG dbPET Image Acquisition

dbPET was performed with FDG (dose range, 101–202 MBq; median, 186 MBq) using the Mammi PET system (Oncovision). Participants fasted for 6 hours prior to imaging, and blood glucose level was measured before intravenous FDG administration. Following an uptake period of 44–56 minutes (median, 44 minutes 36 seconds [IQR, 44 minutes 19 seconds to 44 minutes 57 seconds]; mean, 45 minutes 5 seconds), participants were scanned in a prone position, with a single breast positioned through the aperture into the detector ring. The detector ring translated axially from the nipple toward the chest wall (from anterior to posterior) for approximately 15 minutes, with the number of frames determined by the total length of the breast. dbPET images were reconstructed three-dimensionally using a manufacturer-provided maximum-likelihood expectation-maximization algorithm with a 1-mm kernel and 16 iterations. Attenuation correction was applied using a synthetic CT image created from the dbPET images based on the shape of the breast and the attenuation coefficient of water. The postreconstruction resolution was standardized to 1 × 1 × 1 mm. Both breasts were scanned consecutively in the same imaging session, starting with the breast containing the biopsy-proven tumor.

FDG dbPET Data Analysis

Using OsiriX MD (Pixmeo), we first converted reconstructed images to decay-corrected SUV maps normalized by body weight. Tumors were segmented on converted SUV maps using semiautomated methods based on a region growing algorithm with a threshold of 3 < SUV < 100. The following five parameters were computed within the tumor segmentation using Python version 3.7 (Python Software Foundation) and 3D Slicer version 4.11: *(a)* maximum SUV (SUV_{max}; the maximum uptake value of a single voxel within the tumor segmentation), *(b)* average SUV (SUV_{mean}; the average uptake value of all voxels within the tumor segmentation), *(c)* peak SUV (SUV_{peak}; the average SUV of the voxels within a 1-cm^3 spherical region of interest centered on the voxel with the highest uptake within the tumor segmentation), *(d)* metabolic tumor volume (MTV; the sum of voxel volumes with SUV ≥ 40% of the lesion SUV_{mean}), and *(e)* total lesion glycolysis (TLG; the product of MTV and SUV_{mean}). For each FDG dbPET parameter, percent change at T1 relative to T0 was calculated as $100 \cdot (\text{parameter}_{T1} - \text{parameter}_{T0})/\text{parameter}_{T0}$, where parameter_{T0} and parameter_{T1} are the values at T0 and T1, respectively.

MRI Scan Acquisition

DCE MRI was performed with a 1.5-T scanner (Signa HDxt; GE HealthCare) or a 3-T scanner (SIGNA Premier; GE HealthCare) with a dedicated 16-channel breast coil (Sentinelle). The DCE MRI acquisition protocol was as follows: repetition time/echo time/flip angle, 7 msec/4.2 msec/10° (1.5-T scanner) or 6.7 msec/4.6 msec/12° (3-T scanner); phase acquisition time, 80–100 seconds; field of view, 260–360 mm; in-plane resolution, ≤1 mm; section thickness, ≤2.5 mm; and axial orientation in prone position. Postcontrast images were continuously scanned for six phases. Gadobutrol (Gadavist; Bayer) or gadoterate meglumine (Dotarem; Guerbet) was administered at the manufacturer-recommended dose.

MRI Data Analysis

DCE MRI scans were analyzed using a voxel-based comparison of contrast enhancement of different phases using in-house software developed in Interactive Data Language (L3Harris Geospatial). Early and delayed postcontrast phases were selected from the postcontrast series based on temporal sampling of the center of k-space closest to 2.5 minutes for early phase and 7.5 minutes for late phase. To initiate the MRI measurements, a three-dimensional box region of interest was manually drawn on early phase images to encompass the tumor. Percent enhancement (PE), calculated as $[(S_1 - S_0)/S_0] \cdot 100\%$, and SER, calculated as $(S_1 - S_0)/(S_2 - S_0)$, were computed for each voxel within the region of interest, where S_0, S_1, and S_2 represent the signal intensities on the precontrast, early postcontrast, and late postcontrast images, respectively. MRI-based FTV was then computed as the sum of all voxels meeting the thresholds for PE and SER, which were set as 70% and 0, respectively, based on prior studies (29,30). We defined five different MRI parameters: mean SER (SER_{mean}), peak SER (SER_{peak}), mean PE at early phase (PE_{mean}), peak PE at early phase (PE_{peak}), and FTV. SER_{peak} was measured using automated searching of the entire FTV for the largest mean SER of a connected 8-voxel region (SER hot spot), and SER_{mean} was obtained by averaging the mean SER of the hot spots among all FTV voxels. PE_{peak} and PE_{mean} were measured in a similar manner. For each MRI parameter, percent change at T1 relative to T0 was calculated similarly as for FDG dbPET parameters.

Tumor Characteristics

Ki-67 index and immunohistochemical subtype were pathologically confirmed in the pretreatment core-biopsy specimen. A Ki-67 index cutoff of 20% was previously shown to accurately stratify recurrence and death (31). Therefore, we classified tumors into two groups: high Ki-67 (>20%) and low Ki-67 (≤20%). Using immunohistochemical markers as surrogates for molecular subtypes, we classified tumors into two groups: triple-negative breast cancer (TNBC; ie, HR–/HER2–) and non-TNBC (ie, HR+/HER2+, HR+/HER2–, and HR–/

HER2+). The non-TNBC group was further subdivided into HER2+ and luminal (HR+/HER2–) subtypes for subanalysis.

Histopathologic Outcome and Treatment Response

We used RCB, a histopathologic grading system, to quantify treatment response after NAC on an ordinal scale. RCB is an established surrogate for predicting disease recurrence and survival in patients with breast cancer after NAC (32). RCB classes 0, I, II, and III reflect increasing residual tumor burden in the primary tumor and axillary beds. RCB 0 is equivalent to pathologic complete response. Studies have shown that higher RCB classes accurately identify patients who have poorer prognoses and those who may benefit from additional NAC (33,34). Compared with individuals with RCB 0 or I, those RCB II or III have been shown to have lower survival. Thus, in our study, tumors with an RCB score of II or III at surgical pathology were classified as nonresponsive, whereas those with an RCB score of 0 or I were considered treatment responsive.

Data and Statistical Analysis

We obtained FDG dbPET and DCE MRI parameters at baseline (T0) and 3-week follow-up of NAC (T1). We assessed the association of FDG dbPET and MRI parameters with treatment outcome evaluated by RCB (treatment responsive vs nonresponsive), tumor proliferative activity defined by Ki-67 index (high Ki-67 vs low Ki-67), and pathologic outcome evaluated by subtype (TNBC vs non-TNBC). The absolute value of each parameter was compared between T0 and T1 using the Wilcoxon signed rank test. We focused on the pseudo-median for estimating location because it is the core statistic of the Wilcoxon signed rank test. The pseudo-median is computed as follows: First, the midpoint of every pair of samples is computed (this includes "pairs" where both samples are the same sample). Then, the pseudo-median is the median of the ensuing $n(n + 1)/2$ midpoints. Note that the pseudo-median is the same as the median in the case of symmetric distributions. Comparison of each parameter (absolute value and percent change) between two different groups was done using the Mann-Whitney *U* test (Wilcoxon rank sum test). The Spearman correlation coefficient was used to evaluate the relationship between FDG dbPET and MRI parameters at T0 and T1; the same analysis was repeated in the treatment-responsive and nonresponsive groups. All statistical analyses were performed using R statistical software (version 3.6.3; R Foundation for Statistical Computing). Estimated values are provided with 95% CIs and *P* values. Statistical significance was defined by $P < .05$.

Results

Participant Characteristics

The initial cohort consisted of 20 participants with 22 biopsy-confirmed, locally advanced invasive ductal carcinomas that were imaged in the baseline dbPET and MRI analyses (Fig S1). One participant presented with two distinct tumors in the right breast and one tumor in the left breast. Between baseline and follow-up imaging, five individuals screened out of the I-SPY 2 TRIAL for the following reasons: low-risk disease with triage to neoadjuvant hormonal therapy ($n = 2$), diagnosis of distant metastases ($n = 1$), poor cardiac function ($n = 1$), and patient preference ($n = 1$). Three of the five individuals did not undergo follow-up dbPET, and none of the five individuals underwent follow-up MRI. Overall, for the 3-week follow-up analyses, we included follow-up dbPET in 17 participants with 19 tumors and follow-up MRI in 15 participants with 17 tumors.

Participants in the initial study cohort had a median age of 42.4 years (IQR, 32.0–48.0 years). Seventy-five percent of participants were premenopausal (≤50 years old; 15 of 20), and 25% were postmenopausal (>50 years old; five of 20) (Table). Most tumors were either HR+/HER2– (10 of 22; 45%) or TNBC (seven of 22; 32%). Most participants had positive nodal involvement (12 of 20; 60%) and high baseline Ki-67 (16 of 22; 73%). Following the completion of NAC, surgical pathology revealed that 10 of 21 (48%) tumors (analyzed on a per-breast basis) exhibited a low RCB score (0 or I), and 11 of 21 (52%) had a high RCB score (II or III). The participant with bilateral breast tumors (two on the right and one on the left) had an RCB score of I for the right breast and 0 for the left breast and was therefore included in the treatment-responsive group with respect to all three tumors.

Early Treatment Changes in FDG dbPET and MRI Parameters

FDG dbPET and MRI parameters were compared at baseline (T0) and at follow-up 3 weeks after initiation of treatment (T1) (Fig 1). Statistically significant decreases were observed for all but one of the FDG dbPET parameters after 3 weeks of NAC (pseudo-median difference [95% CI]) (Fig 1A–1E): SUV_{max}, −6.2 (−10.2, −2.6; $P < .001$); SUV_{mean}, −2.6 (−4.9, −1.3; $P < .001$); SUV_{peak}, −4.2 (−6.9, −2.3; $P < .001$), and TLG, −29.1 mL^3 (−71.4, −6.8; $P = .005$). There was no evidence of a difference in MTV after NAC (2.3 mL^3 [−0.2, 5.1]; $P = .06$).

An early change was also observed in MRI parameters (Fig 1F–1J). Statistically significant decreases in MRI measures of SER_{peak} (pseudo-median difference, −1.0 [95% CI: −1.3, −0.2]; $P = .02$) and FTV (−11.6 mL^3 [−22.2, −1.7]; $P = .009$) were observed at T1 relative to T0, with no evidence of a difference in SER_{mean} (−0.2 [−0.7, 0.1]; $P = .20$) or PE_{mean} (−13.2% [−56.0%, 30.9%]; $P = .54$) between the two time points.

Association between FDG dbPET and MRI Parameters and Pathologic Outcome Evaluated Using RCB

Absolute value at T0— There was no evidence of a difference between treatment-responsive (RCB score 0 or I) and nonresponsive tumors (RCB score II or III) in baseline TLG (difference, 62.1 mL^3 [95% CI: −8.1, 138.4]; $P = .10$) or MTV (5.9 mL^3 [0.0, 16.5]; $P = .05$) (Fig S2D, S2E). There was no apparent relationship between treatment response and baseline SUV measures (Fig S2A–S2C) or baseline MRI parameters (Fig S2F–S2J).

Percent change from T0 to T1— Figures 2 and 3 show example dbPET and MR images in participants with tumors classified as treatment-responsive and nonresponsive, respectively. For

Summary of Participant and Tumor Characteristics

Characteristic	Value
No. of participants	20
Age (y)*	42.4 (32.0–48.0)
Body weight (kg)*	69.4 (62.4–72.6)
Body mass index*†	25.9 (23.4–27.0)
Lean body mass (kg)*	47.1 (44.2–49.1)
Menopause status	
Premenopause (≤50 y old)	15
Postmenopause (>50 y old)	5
Tumor characteristics	
No. of unique tumors	22
Stage	
I	1
II	8
III	12
IV	1
Tumor subtype	
ER+/PR+/HER2+	2
ER+/PR+/HER2−	10
ER−/PR−/HER2+	3
ER−/PR−/HER2−	7
Nodal status‡	
With positive involvement	12 (60)
Without positive involvement	8 (40)
Tumor molecular characteristics	
Baseline Ki-67	
Low (≤20%)	6
High (>20%)	16
Pathologic complete response§	7
Residual cancer burden§	
Low (0 or I)	10
High (II or III)	11

Note.—Unless otherwise indicated, participant characteristics are presented as the number of participants, and tumor characteristics are presented as the number of tumors. ER = estrogen receptor, HER2 = human epidermal growth factor receptor 2, PR = progesterone receptor.
* Values are presented as medians (IQRs).
† Calculated as weight in kilograms divided by height in meters squared.
‡ Values are presented as numbers of participants, with percentages in parentheses.
§ Values are presented as numbers of tumors on a per-breast basis (one participant had two tumors in the right breast and one tumor in the left breast).

both FDG dbPET and MRI parameters, there was no evidence of a difference in estimated percent decrease from T0 to T1 between the treatment-responsive and nonresponsive groups. Relative to the nonresponsive group, the responsive group showed the following differences (95% CIs) in percent change in FDG dbPET parameters: SUV_{max}, −34.3% (−55.9%, 1.5%; P = .06); SUV_{mean}, −18.8% (−49.1%, 23.0%; P = .27); SUV_{peak}, −27.7% (−51.6%, 8.5%; P = .21); TLG, −25.1% (−83.7%, 15.8%; P = .06); and MTV, −31.9% (−109.6%, 15.0%; P = .13) (Fig 4A–4E). Relative to the nonresponsive group, the responsive group showed the following differences (95% CIs) in percent change in MRI parameters: PE_{peak}, −42.4% (−110.5%, 8.5%; P = .08) and PE_{mean}, −20.9% (−85.9%, 17.9%; P = .31) (Fig 4F, 4G). There was no evidence of a difference between the two groups in the other MRI measures: SER_{mean}, −5.5% (−39.7%, 30.3%; P = .79); SER_{peak}, 0% (−44.7%, 22.0%; P = .69); and FTV, −8.3% (−68.4%, 30.9%; P = .54) (Fig 4H–4J).

Relationship between FDG dbPET and MRI Parameters and Ki-67 Index

Absolute value at T0— Tumors with high Ki-67 index (high Ki-67 group) had statistically significantly higher estimated baseline FDG dbPET values of SUV_{mean} (difference, 5.1 [95% CI: 0.4, 6.9]; P = .01) and SUV_{peak} (5.5 [0.9, 10.5]; P = .04) than tumors in the low Ki-67 group (Fig 5B, 5C). There was no evidence of a difference in estimated baseline SUV_{max} (difference, 10.8 [95% CI: −28.7, 18.6]; P = .09), TLG (24.3 [−676.4, 144.1]; P = .31), or MTV (0.2 mL^3 [−58.3, 16.1]; P = .84) between the two groups (Fig 5A, 5D, 5E).

There was no evidence of a difference in the estimated baseline MRI parameters between the high Ki-67 and low Ki-67 groups for PE_{peak} (difference, 46.5% [95% CI: −143.5%, 176.1%]; P = .49), PE_{mean} (29.4% [−116.3%, 117.3%]; P = .54), FTV (5.5 mL^3 [−14.6, 38.7]; P = .54), SER_{peak} (0 [0.0, 0.2]; P = .64), or SER_{mean} (−0.1 [−0.8, 0.7]; P = .77) (Fig 5F–5J).

Percent change from T0 to T1— After 3 weeks of treatment, relative to the low Ki-67 group, the high Ki-67 group showed the following differences (95% CIs) in percent change in FDG dbPET parameters: SUV_{max}, −29.5% (−62.8%, 7.1%; P = .15); SUV_{mean}, −19.7% (−50.5%, 13.1%; P = .18); SUV_{peak}, −23.6% (−56.7%, 8.6%; P = .18); TLG, −38.2% (−146.8%, 28.6%; P = .18); and MTV, −28.2% (−156.7%, 38.1%; P = .41) (Fig S3A–S3E).

After 3 weeks of treatment, relative to the low Ki-67 group, the high Ki-67 group showed the following differences (95% CIs) in percent change in MRI parameters: FTV, −15.6% (−97.7%, 51.9%; P = .77); PE_{peak}, −18.6% (−104.9%, 54.5%; P = .59); SER_{peak}, −14.6% (−51.2%, 22.0%; P = .46); and SER_{mean}, −13.6% (−54.9%, 48.4%; P = .50) (Fig S3G–S3J). There was no evidence of a difference between the high and low Ki-67 groups in percent change in PE_{mean} (−0.2% [−45.5%, 72.1%]; P > .99) (Fig S3F).

Association between FDG dbPET and MRI Parameters and Immunohistochemical Subtype

Absolute value at T0— There was no evidence of a difference between the TNBC and non-TNBC groups in baseline SUV_{max} (difference, 5.3 [95% CI: −6.9, 13.5]; P = .33), SUV_{mean} (0.7 [−2.4, 5.7]; P = .63), SUV_{peak} (2.2 [−3.5, 8.6]; P = .78), TLG (17.9 [−65.0, 160.8]; P = .54), or MTV (0.4 mL^3 [−7.6, 17.3]; P = .78) (Fig S4A–S4E). In the subanalysis in which the non-TNBC group was further divided into HER2+ and luminal subtypes, no statistical analysis was performed because of the small sample size, but the results suggest no remarkable differ-

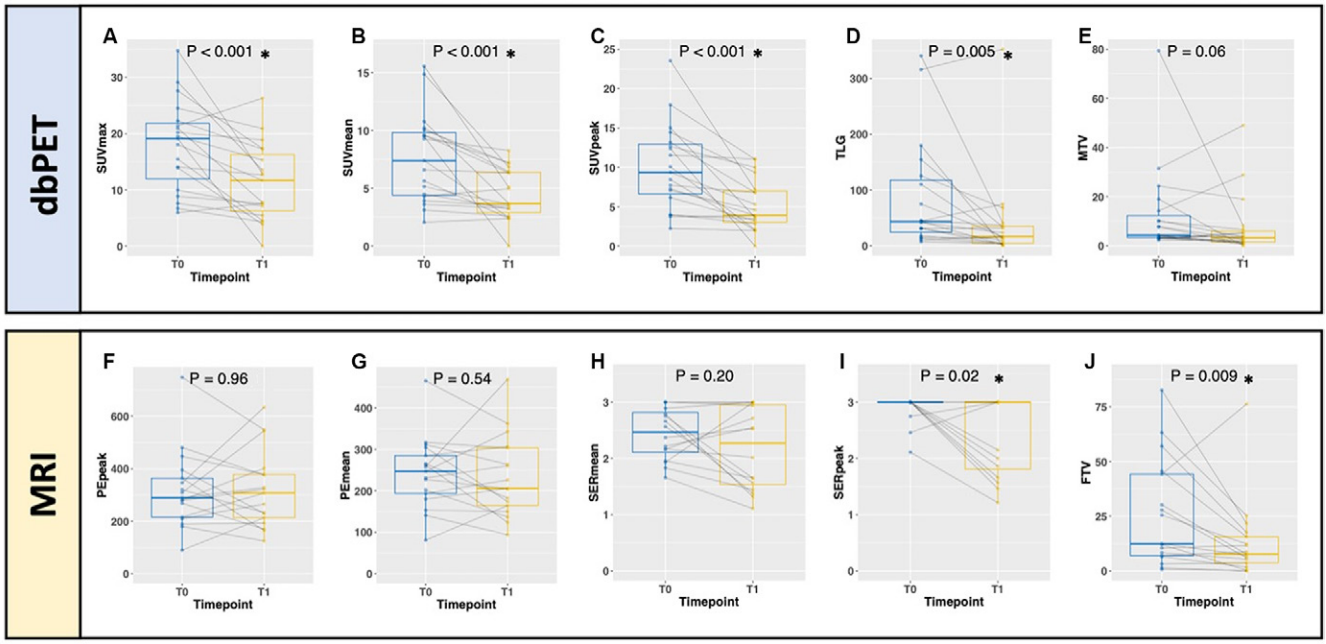

Figure 1: Box-and-whisker plots show comparison of parameters of fluorine 18 fluorodeoxyglucose uptake at dedicated breast PET (dbPET) and MRI parameters of the same lesion at T0 (week 0) and T1 (week 3). **(A–E)** dbPET parameters: **(A)** maximum standardized uptake value (SUV), **(B)** mean SUV, **(C)** peak SUV, **(D)** total lesion glycolysis (TLG), and **(E)** metabolic tumor volume (MTV). **(F–J)** MRI parameters: **(F)** peak percent enhancement (PE), **(G)** mean PE, **(H)** mean signal enhancement ratio (SER), **(I)** peak SER, and **(J)** functional tumor volume (FTV). The boundaries of the boxes indicate the lower and upper quartiles, the lines within the boxes indicate the medians, and the whiskers indicate the range (not including outliers). Gray lines connect the data for individual lesions. * = $P < .05$.

ences in the distribution of baseline FDG dbPET parameters for each subtype (Fig S5A–S5E).

At baseline, there was no evidence of a difference between the TNBC and non-TNBC groups in the MRI parameters of PE_{peak} (difference, −30.6% [95% CI: −157.5%, 95.2%]; P = .73), PE_{mean} (−27.3% [−116.3%, 51.0%]; P = .78), FTV (−6.2 mL^3 [−31.1, 9.0]; P = .41), SER_{peak} (0 [−0.2, 0.0]; P = .67), or SER_{mean} (−0.2 [−0.8, 0.3]; P = .40) (Fig S4F–S4J). In the subanalysis in which the non-TNBC group was further divided into HER2+ and luminal subtypes, no statistical analysis was performed because of the small sample size, but the results suggest no remarkable differences in the distribution of baseline MRI parameters for each subtype (Fig S5F–S5J).

Percent change from T0 to T1— After 3 weeks of treatment, FDG dbPET parameters showed the following differences (95% CIs) in percent change from T0 to T1 in the TNBC versus the non-TNBC group: SUV_{max}, 8.7% (−21.2%, 49.1%; P = .57); SUV_{mean}, 18.1% (−24.0%, 46.4%; P = .41); SUV_{peak}, 13.2% (−14.2%, 43.6%; P = .17); TLG, 19% (−42.5%, 75.2%; P = .52); and MTV, 31.6% (−30.4%, 108.6%; P = .36) (Fig 6A–6E). In the subanalysis further dividing the non-TNBC group into HER2+ and luminal subtypes, no statistical analysis was performed because of small sample size, but the results suggest the possibility that HER2+ tumors had greater estimated declines in FDG dbPET parameters compared with luminal subtype and TNBC tumors after 3 weeks of neoadjuvant treatment (Fig S6A–S6E).

At MRI, TNBCs showed the following differences (95% CIs) relative to non-TNBCs in percent change from T0 to T1: FTV, 40.9% (−7.8%, 107.5%; P = .14); PE_{mean}, 28.6% (−9.5%, 71.0%; P = .12); PE_{peak}, 24.0% (−39.8%, 70.7%; P = .30); SER_{peak}, −14.6% (−51.2%, 22.0%; P = .77); and SER_{mean}, −13.6% (−54.9%, 48.4%; P = .63) (Fig 6F–6J). In the subanalysis further dividing the non-TNBC group into HER2+ and luminal subtypes, no statistical analysis was performed because of the small sample size, but the results suggest the possibility that the HER2+ group had larger estimated decreases in MRI parameters, particularly PE and FTV, compared with the TNBC and luminal subtype groups (Fig S6F–S6J).

Correlation of Fluorine 18 FDG dbPET and Breast MRI Measures at Baseline and during Early Treatment

FDG dbPET parameters were plotted against breast MRI parameters at baseline and follow-up. Baseline PE_{peak} was correlated with baseline SUV_{max} (Spearman ρ = 0.60 [95% CI: 0.01, 0.85]; P = .004) (Fig 7A). Baseline PE_{mean} was correlated with baseline SUV_{max} (ρ = 0.57 [95% CI: −0.05, 0.83]; P = .006) (Fig 7B). Baseline values of FTV and MTV were also correlated (ρ = 0.53 [95% CI: −0.4, 0.80], P = .01) (Fig 7C).

Similar relationships between dbPET and MRI parameters were observed at follow-up imaging at T1. PE_{peak} and PE_{mean} were correlated with SUV_{max} (PE_{peak}, ρ = 0.51 [95% CI: −0.03, 0.80], P = .03; PE_{mean}, 0.54 [0.04, 0.82], P = .02) (Fig 7G, 7H). PE_{mean} was also correlated with SUV_{mean} (ρ = 0.51 [95% CI: 0.06, 0.79]; P = .04) and SUV_{peak} (0.51 [−0.01, 0.78]; P = .04) (Fig S7K, S7L). There was no apparent correlation between FTV and MTV at T1 (Fig 7I).

Feature correlations at T0 and T1 were also calculated based on treatment response status (Figs 7D–7F, 7J–7L, S7E–S7H, S7M–S7P). Responding tumors demonstrated the strongest correlations between dbPET and MRI features at T0 and T1.

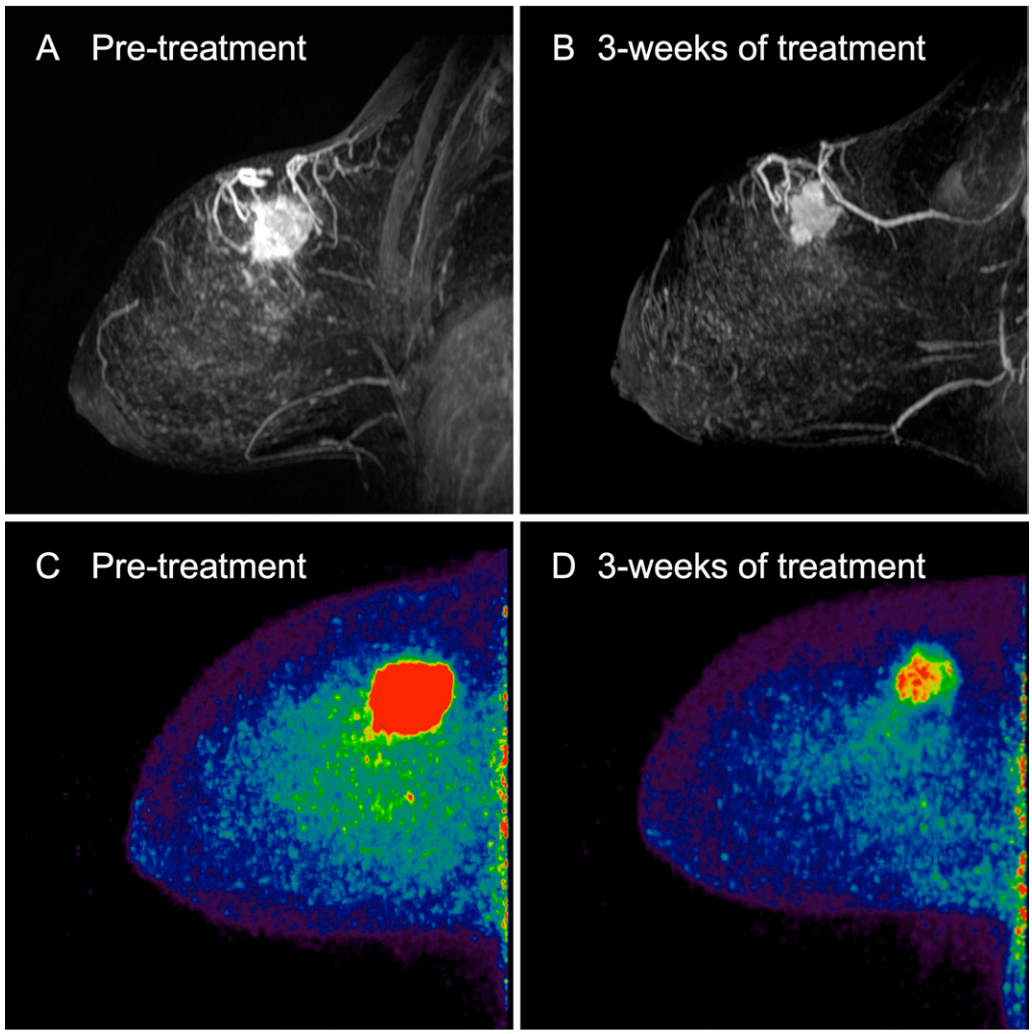

Figure 2: Images in a 27-year-old participant with triple-negative right breast cancer who was classified as having a treatment-responsive tumor (residual cancer burden class 0). **(A, B)** Sagittal maximum intensity projection postcontrast T1-weighted MRI scans show decrease in enhancing tumor volume from **(A)** baseline to **(B)** 3 weeks after treatment. **(C, D)** Sagittal maximum intensity projection dedicated breast PET images show decrease in fluorine 18 fluorodeoxyglucose uptake from **(C)** baseline to **(D)** 3 weeks after treatment.

Discussion

Studies have shown that both FDG PET and breast MRI can predict early response to NAC. However, neither technique alone has demonstrated sufficiently high accuracy in identifying nonresponding tumors early in the course of NAC to direct changes in clinical management. Preliminary research has shown that combined evaluation with wbPET and MRI may improve prediction accuracy in early treatment (14,35,36). In our pilot study, we explored the potential of high-resolution dbPET to further complement MRI evaluation during early treatment. Consistent with prior studies of wbPET (14), dbPET measures were overall more sensitive to early treatment response than MRI. We observed statistically significant decreases in nearly all FDG dbPET measures 3 weeks after the initiation of NAC. Among MRI measures, only FTV and SER_{peak} showed statistically significant decreases during early treatment, findings that are also consistent with previous studies (11).

Stratification of tumors into treatment-responsive and nonresponsive groups based on RCB permitted us to evaluate whether early changes in FDG dbPET and MRI measures correlated with the overall treatment response. We observed potentially larger decreases in all of the dbPET measures (vs only a subset of MRI measures) in treatment-responsive relative to nonresponsive tumors. Although these differences were not statistically significant, they are likely to be clinically relevant given the large magnitude of potential differences. While further validation is needed, we hypothesize that the higher sensitivity and greater dynamic range of dbPET relative to wbPET may facilitate discrimination between responsive and nonresponsive tumors in the early treatment setting. Future larger prospective studies with well-defined cohorts are needed to determine whether multiparametric imaging evaluation using FDG dbPET and MRI may aid in the prediction of responsiveness to neoadjuvant treatments.

Unlike DCE MRI, which is sensitive to blood volume and vascular permeability, FDG dbPET reflects tissue metabolism. Ki-67, a nuclear protein correlating with the degree of cellular proliferation, is often used as a prognostic biomarker to guide treatment decisions and track treatment response in breast

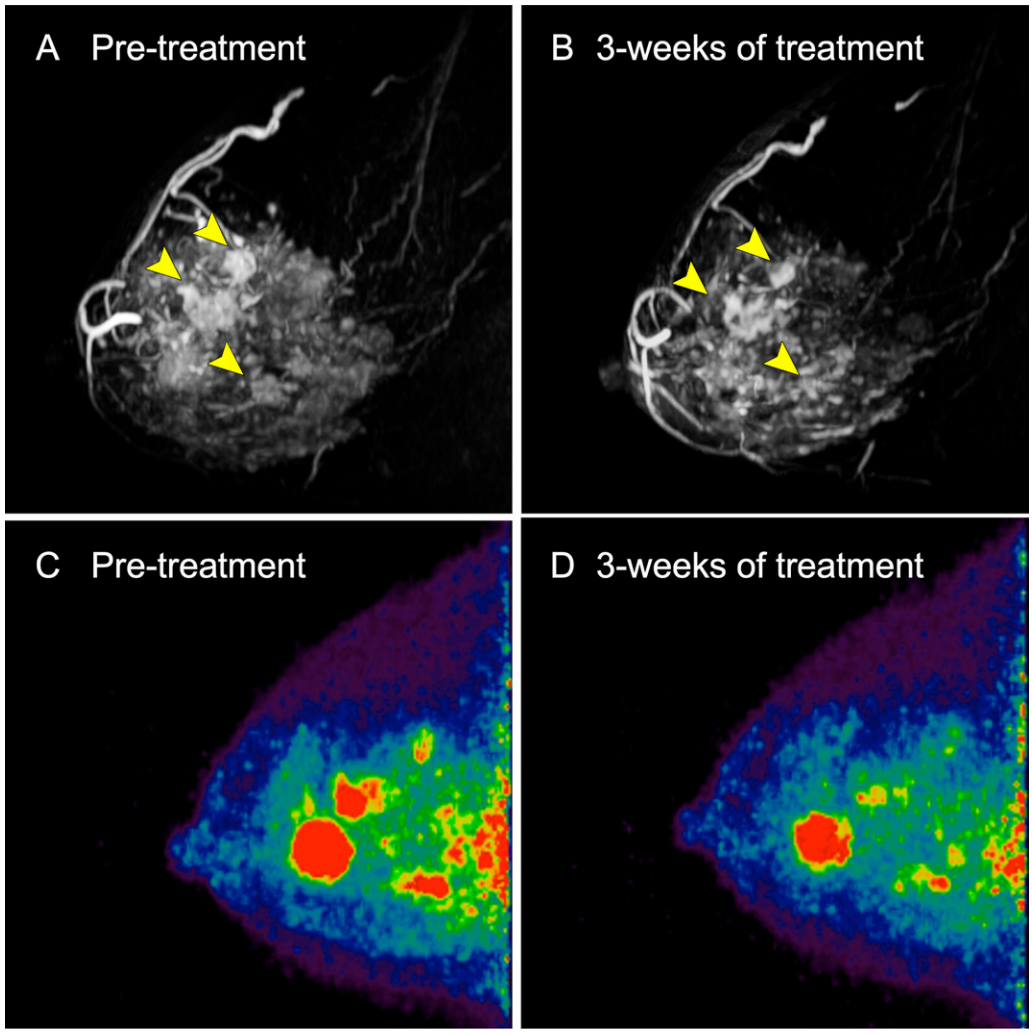

Figure 3: Images in a 42-year-old participant with estrogen receptor–positive/progesterone receptor–positive/human epidermal growth factor receptor 2–negative multifocal right breast cancer who was classified as a having a nonresponsive tumor (residual cancer burden class 3). **(A, B)** Sagittal maximum intensity projection postcontrast T1-weighted MRI scans show a decrease in the volume of multifocal enhancing masses (arrowheads) from **(A)** baseline to **(B)** 3 weeks after treatment. **(C, D)** Sagittal maximum intensity projection dedicated breast PET images show a corresponding decrease in multifocal fluorine 18 fluorodeoxyglucose uptake from **(C)** baseline to **(D)** 3 weeks after treatment.

cancer (37). When we dichotomized tumors into high and low Ki-67 groups, we found that high Ki-67 tumors had significantly higher SUV at baseline compared with low Ki-67 tumors. Furthermore, tumors with high baseline Ki-67 levels exhibited a tendency toward greater decreases in all dbPET parameters after 3 weeks of NAC, though no differences reached statistical significance. These observations suggest that dbPET parameters may be correlated with tumor proliferation, which in turn reflects the likelihood of response to NAC.

Given previous studies showing differences in signs of treatment response at both MRI and PET based on receptor status (11,38–41), we sought to compare MRI and FDG dbPET parameters between TNBC and non-TNBC tumors. Concordant with the literature, our results showed potentially higher baseline FDG dbPET parameters in TNBC compared with non-TNBC tumors, reflecting the higher proliferative index and aggressiveness of TNBC (22). After 3 weeks of treatment, TNBCs showed a more modest potential decrease in FDG dbPET parameters compared with non-TNBCs, despite the fact that TNBCs had the higher rate of RCB in our data set. However, on further analysis, the potentially greater decrease in FDG dbPET parameters in the non-TNBC group was shown to be possibly due to the HER2+ subgroup, which had a similarly high rate of RCB in our data set. Finally, the non-TNBC group showed potentially higher percent decreases in volumetric dbPET measures (TLG and MTV) than in dbPET SUVs, suggesting that volumetric measures may be more sensitive in capturing treatment response in non-TNBCs. This could be related to non-TNBCs having lower metabolic activity at baseline than TNBCs and is consistent with other published studies (12,42,43).

We expected to see greater reductions in MRI measures of tumor volume and enhancement for TNBCs relative to non-TNBCs, given the higher rates of treatment response of TNBCs, especially compared with the luminal subtype, which had the lowest rate of RCB. However, we instead observed a potentially

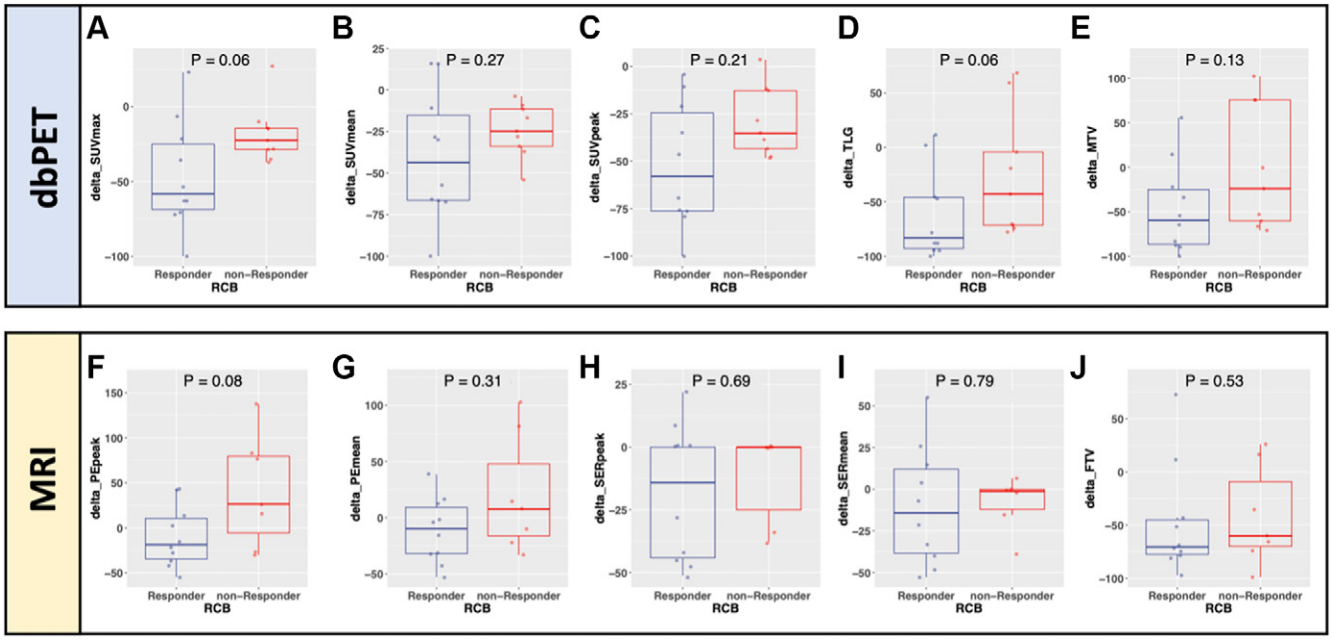

Figure 4: Box-and-whisker plots show comparison of the change between T0 and T1 (delta) in parameters of fluorine 18 fluorodeoxyglucose uptake at dedicated breast PET (dbPET) and MRI parameters in treatment-responsive and nonresponsive groups determined by residual cancer burden (RCB). **(A–E)** dbPET parameters: **(A)** maximum standardized uptake value (SUV), **(B)** mean SUV, **(C)** peak SUV, **(D)** total lesion glycolysis (TLG), and **(E)** metabolic tumor volume (MTV). **(F–J)** MRI parameters: **(F)** peak percent enhancement (PE), **(G)** mean PE, **(H)** mean signal enhancement ratio (SER), **(I)** peak SER, and **(J)** functional tumor volume (FTV). The boundaries of the boxes indicate the lower and upper quartiles, the lines within the boxes indicate the medians, and the whiskers indicate the range (not including outliers).

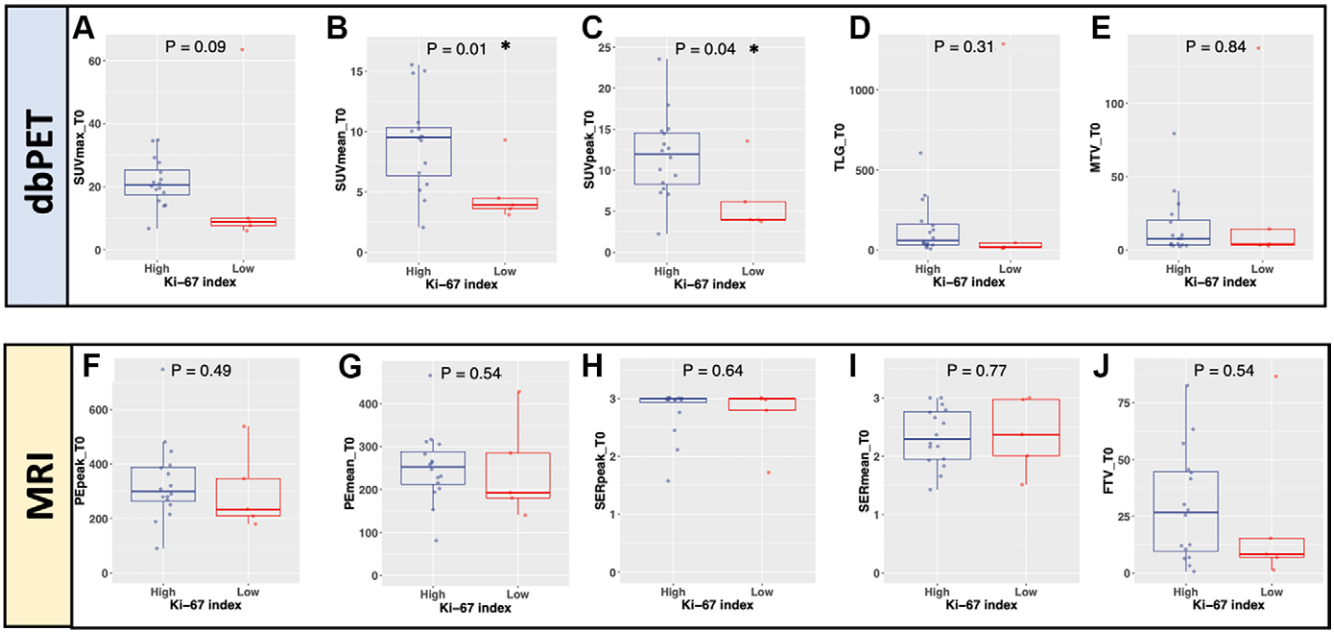

Figure 5: Box-and-whisker plots show comparison of parameters of fluorine 18 fluorodeoxyglucose uptake at dedicated breast PET (dbPET) and MRI parameters at baseline (T0) between the high Ki-67 and low Ki-67 groups. **(A–E)** dbPET parameters: **(A)** maximum standardized uptake value (SUV), **(B)** mean SUV, **(C)** peak SUV, **(D)** total lesion glycolysis (TLG), and **(E)** metabolic tumor volume (MTV). **(F–J)** MRI parameters: **(F)** peak percent enhancement (PE), **(G)** mean PE, **(H)** peak signal enhancement ratio (SER), **(I)** mean SER, and **(J)** functional tumor volume (FTV). The boundaries of the boxes indicate the lower and upper quartiles, the lines within the boxes indicate the medians, and the whiskers indicate the range (not including outliers). * = $P < .05$.

greater reduction in MRI FTV in the non-TNBC group. One possible explanation is that baseline tumor volumes in the non-TNBC group may have been overestimated due to background parenchymal enhancement (BPE). In general, TNBCs tend to be more well-defined masses in comparison to non-TNBCs, which may be infiltrative or multifocal and hence more difficult to distinguish from surrounding BPE. Since BPE tends to decline with the initiation of neoadjuvant therapy, the apparent reduction in non-TNBC tumor volume in early treatment could, in part, reflect a reduction in BPE. This phenomenon was observed previously in the I-SPY 1 TRIAL (11,38,44), in which the change in MRI FTV relative to baseline was less predictive of

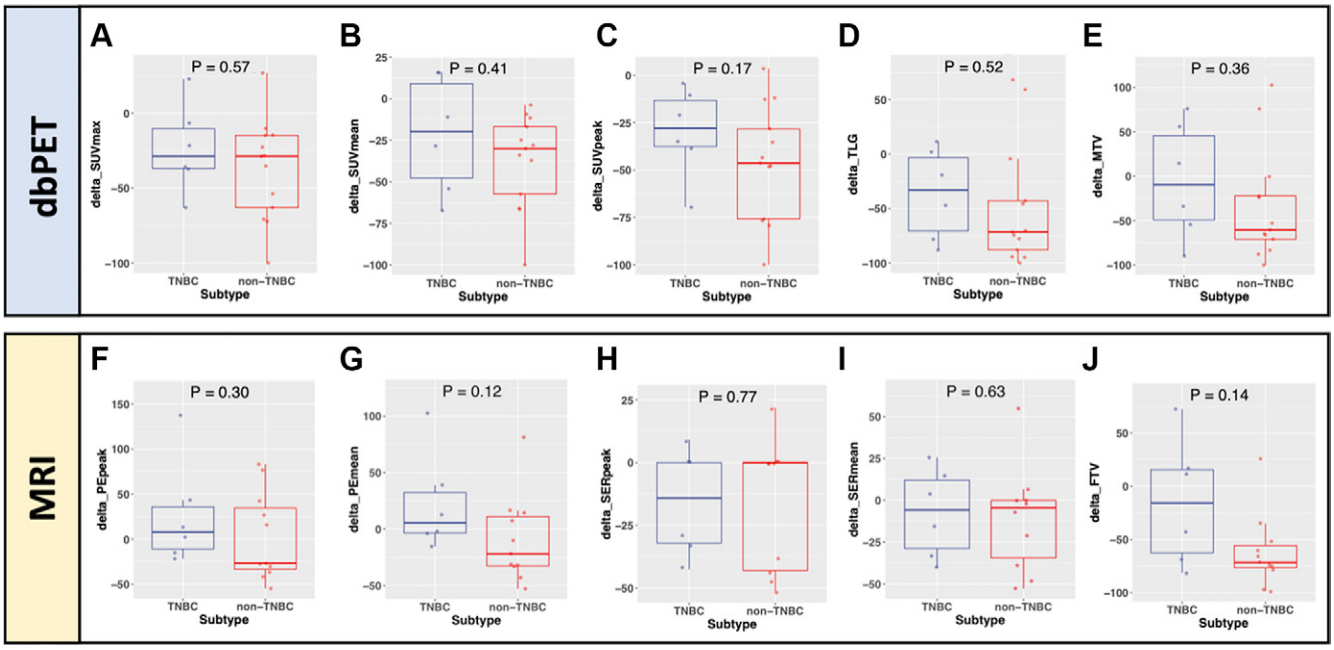

Figure 6: Box-and-whisker plots show comparison of the change between T0 and T1 (delta) in parameters of fluorine 18 fluorodeoxyglucose uptake at dedicated breast PET (dbPET) and MRI parameters in participants with triple-negative breast cancer (TNBC) and non-TNBC. **(A–E)** dbPET parameters: **(A)** maximum standardized uptake value (SUV), **(B)** mean SUV, **(C)** peak SUV, **(D)** total lesion glycolysis (TLG), and **(E)** metabolic tumor volume (MTV). **(F–J)** MRI parameters: **(F)** peak percent enhancement (PE), **(G)** mean PE, **(H)** mean signal enhancement ratio (SER), **(I)** peak SER, and **(J)** functional tumor volume (FTV). The boundaries of the boxes indicate the lower and upper quartiles, the lines within the boxes indicate the medians, and the whiskers indicate the range (not including outliers).

treatment response and survival outcomes than other measures, owing to uncertainty in baseline volume measurements. Since BPE may confound MRI evaluation of treatment response at early time points, this suggests a complementary role for FDG dbPET, although further studies are needed to address whether background parenchymal uptake may similarly confound dbPET evaluation (45–47).

Correlation analysis between dbPET and MRI features suggests that baseline SUVs, particularly SUV_{max}, and the dbPET volumetric feature MTV are moderately correlated with MRI PE and FTV, respectively. Furthermore, the correlations between dbPET and MRI measures are improved when considering only tumors responsive to treatment. This is consistent with previous studies demonstrating that mismatches between perfusion and metabolism are associated with poor responses to therapy (48). At 3 weeks, the relationship between SUV and PE was preserved, but not that between MTV and FTV. The lack of correlation between MRI and dbPET measures after treatment could be attributed to the differential effects of NAC on metabolism and perfusion, as well as the fact that metabolic changes tend to precede anatomic changes. Thus, the weaker correlation between modalities after initiation of therapy is to be expected, as each technique offers distinct information in the early assessment of tumor response.

Limitations of our study include the fact that the I-SPY 2 TRIAL inclusion criteria restricted our analysis to tumors larger than 2.5 cm in participants with advanced stage (II/III) cancer undergoing treatment at a single institution, which may not represent the general breast cancer population. Furthermore, we recruited volunteers from among participants enrolling in the I-SPY 2 TRIAL at our institution to undergo dbPET imaging. Since the participants in our study were not randomized, this introduced selection bias. We are also unable to report whether the participants in the study received standard versus experimental therapies because this information has not yet been published by the I-SPY 2 TRIAL drug team. A final major limitation of our study relates to our small participant cohort, with limited statistical power to detect differences in dbPET and MRI measures following NAC. This was even more pronounced for the subgroup analyses based on RCB status, histopathologic data, and immunohistochemical subtypes. Due to the exploratory nature of this study, no adjustment was made for multiple hypothesis testing, although this would be warranted in future larger studies. As such, our findings should be viewed as preliminary and hypothesis generating rather than conclusive.

In this pilot study, we demonstrated the potential of dbPET to provide complementary information to MRI during early neoadjuvant therapy. Based on the current evidence, it is uncertain whether dbPET, MRI, or a combination of these techniques is most accurate for early treatment evaluation, and there remains a clinical need for better image-based tools to predict response or nonresponse. Cost-benefit analyses will also be necessary to determine whether the clinical benefit and cost savings of avoiding ineffective treatments justify the costs incurred by these advanced imaging techniques. Incorporation of dbPET along with breast MRI into larger multicenter prospective neoadjuvant treatment trials will be needed to ensure adequate power to evaluate outcomes by molecular subtype. An advantage of dbPET technology is the ability to incorporate receptor-specific radiotracers in these neoadjuvant trial paradigms for the development of imaging biomarkers to further support precision treatment of breast cancer.

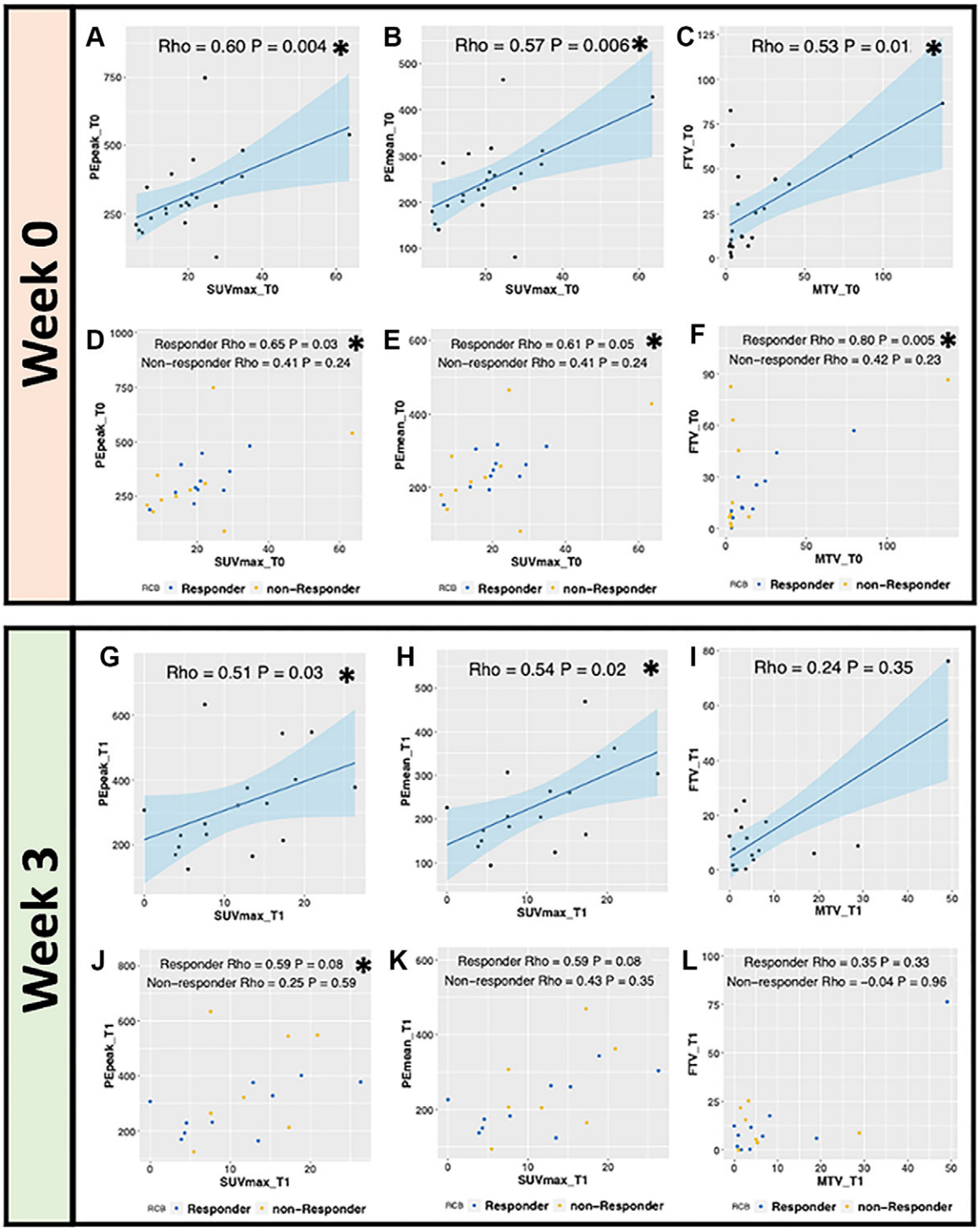

Figure 7: Correlation plots between fluorine 18 fluorodeoxyglucose dedicated breast PET (x-axis) and MRI (y-axis) parameters at **(A–F)** T0 and **(G–L)** T1 and for all participants (**[A–C]** and **[G–I]**) and stratified by responder status (**[D–F]** and **[J–L]**). **(A)** Baseline maximum standardized uptake value (SUV) versus peak percent enhancement (PE); **(B)** baseline maximum SUV versus mean PE; **(C)** baseline metabolic tumor volume (MTV) versus functional tumor volume (FTV); **(D–F)** as in **A–C** but with responsive group in blue and nonresponsive group in yellow; **(G)** maximum SUV versus peak PE at T1; **(H)** maximum SUV versus mean PE at T1; **(I)** MTV versus FTV at T1; **(J–L)** as in **G–I** but with responsive group in blue and nonresponsive group in yellow. Rho = Spearman correlation coefficient, * = $P < .05$.

Acknowledgments: The authors would like to thank all patients who participated in the I-SPY 2 TRIAL, working group chairs, investigators, and study coordinators from all participant sites for their contributions to the project. This work was prepared while E.F.J. was employed at the University of California San Francisco. The opinions expressed in this article are the authors' own and do not reflect the view of the National Institutes of Health, the Department of Health and Human Services, or the United States government.

Author contributions: Guarantors of integrity of entire study, **D.D., N.M.H., K.M.R.**; study concepts/study design or data acquisition or data analysis/interpretation, all authors; manuscript drafting or manuscript revision for important intellectual content, all authors; approval of final version of submitted manuscript, all authors; agree to ensure any questions related to the work are appropriately resolved, all authors; literature research, **D.D., N.O., B.N.J., E.F.J., K.M.R.**; clinical studies, **D.D., D.K.H., C.L.H., R.G., J.M.V., R.R.F., L.J.E., B.N.J., N.M.H., E.F.J.,**

K.M.R.; statistical analysis, **D.D., N.O., J.K., L.J.E., E.F.J.**; and manuscript editing, **D.D., N.O., C.L.H., J.K., W.L., Y.S., R.R.F., D.H., L.J.E., B.N.J., N.M.H., E.F.J., K.M.R.**

Data sharing: Data generated by the authors or analyzed during the study are available at: https://wiki.cancerimagingarchive.net/pages/viewpage.action?pageId=70230072.

Disclosures of conflicts of interest: **D.D.** No relevant relationships. **N.O.** No relevant relationships. **D.K.H.** Employed by and owns stock in Regeneron Pharmaceuticals. **C.L.H.** No relevant relationships. **J.K.** No relevant relationships. **W.L.** No relevant relationships. **R.G.** No relevant relationships. **J.M.V.** No relevant relationships. **Y.S.** No relevant relationships. **R.R.F.** No relevant relationships. **D.H.** No relevant relationships. **S.B.** No relevant relationships. **L.J.E.** Involved in investigator-initiated trial for high-risk ductal carcinoma in situ funded by Moderna for ductal carcinoma in situ phase I study; uncompensated board member for Quantum Leap Healthcare Collaborative, which provides funding to University of California San Francisco, for the I-SPY TRIAL; payment from UpToDate for editing medical materials; member of Blue Cross Blue Shield medical advisory panel and travel reimbursement from Blue Cross Blue Shield for attending medical advisory panel meeting. **B.N.J.** Author royalties from UpToDate; honoraria for lectures from the American College of Radiology, World Class CME, and Medscape; travel reimbursement for attending meetings from RSNA, American College of Radiology, National Diagnostic Imaging Symposium, and Medscape; member of the board of trustees of the RSNA Research and Education Foundation; and deputy editor for *Radiology: Imaging Cancer*. **N.M.H.** Member of RSNA Science Council. **E.F.J.** No relevant relationships. **K.M.R.** No relevant relationships.

References

1. Polyak K. Heterogeneity in breast cancer. J Clin Invest 2011;121(10):3786–3788.
2. van 't Veer LJ, Dai H, van de Vijver MJ, et al. Gene expression profiling predicts clinical outcome of breast cancer. Nature 2002;415(6871):530–536.
3. Waks AG, Winer EP. Breast cancer treatment: a review. JAMA 2019;321(3):288–300.
4. Russnes HG, Navin N, Hicks J, Borresen-Dale AL. Insight into the heterogeneity of breast cancer through next-generation sequencing. J Clin Invest 2011;121(10):3810–3818.
5. Perou CM, Sørlie T, Eisen MB, et al. Molecular portraits of human breast tumours. Nature 2000;406(6797):747–752.
6. Foulkes WD, Smith IE, Reis-Filho JS. Triple-negative breast cancer. N Engl J Med 2010;363(20):1938–1948.
7. Korde LA, Somerfield MR, Carey LA, et al. Neoadjuvant chemotherapy, endocrine therapy, and targeted therapy for breast cancer: ASCO guideline. J Clin Oncol 2021;39(13):1485–1505.
8. Reig B, Lewin AA, Du L, et al. Breast MRI for evaluation of response to neoadjuvant therapy. RadioGraphics 2021;41(3):665–679.
9. Kong X, Moran MS, Zhang N, Haffty B, Yang Q. Meta-analysis confirms achieving pathological complete response after neoadjuvant chemotherapy predicts favourable prognosis for breast cancer patients. Eur J Cancer 2011;47(14):2084–2090.
10. Cortazar P, Zhang L, Untch M, et al. Pathological complete response and long-term clinical benefit in breast cancer: the CTNeoBC pooled analysis. Lancet 2014;384(9938):164–172. [Published correction appears in Lancet 2019;393(10175):986.]
11. Hylton NM, Blume JD, Bernreuter WK, et al. Locally advanced breast cancer: MR imaging for prediction of response to neoadjuvant chemotherapy—results from ACRIN 6657/I-SPY TRIAL. Radiology 2012;263(3):663–672.
12. Groheux D, Giacchetti S, Delord M, et al. 18F-FDG PET/CT in staging patients with locally advanced or inflammatory breast cancer: comparison to conventional staging. J Nucl Med 2013;54(1):5–11.
13. Mghanga FP, Lan X, Bakari KH, Li C, Zhang Y. Fluorine-18 fluorodeoxyglucose positron emission tomography-computed tomography in monitoring the response of breast cancer to neoadjuvant chemotherapy: a meta-analysis. Clin Breast Cancer 2013;13(4):271–279.
14. Sheikhbahaei S, Trahan TJ, Xiao J, et al. FDG-PET/CT and MRI for evaluation of pathologic response to neoadjuvant chemotherapy in patients with breast cancer: a meta-analysis of diagnostic accuracy studies. Oncologist 2016;21(8):931–939.
15. Wang Y, Zhang C, Liu J, Huang G. Is 18F-FDG PET accurate to predict neoadjuvant therapy response in breast cancer? A meta-analysis. Breast Cancer Res Treat 2012;131(2):357–369.
16. Groves AM, Shastry M, Rodriguez-Justo M, et al. [18]F-FDG PET and biomarkers for tumour angiogenesis in early breast cancer. Eur J Nucl Med Mol Imaging 2011;38(1):46–52.
17. Semple SI, Gilbert FJ, Redpath TW, et al. The relationship between vascular and metabolic characteristics of primary breast tumours. Eur Radiol 2004;14(11):2038–2045.
18. García Vicente AM, Soriano Castrejón Á, León Martín A, et al. Molecular subtypes of breast cancer: metabolic correlation with [18]F-FDG PET/CT. Eur J Nucl Med Mol Imaging 2013;40(9):1304–1311.
19. Bolouri MS, Elias SG, Wisner DJ, et al. Triple-negative and non-triple-negative invasive breast cancer: association between MR and fluorine 18 fluorodeoxyglucose PET imaging. Radiology 2013;269(2):354–361.
20. Connolly RM, Leal JP, Goetz MP, et al. TBCRC 008: early change in 18F-FDG uptake on PET predicts response to preoperative systemic therapy in human epidermal growth factor receptor 2-negative primary operable breast cancer. J Nucl Med 2015;56(1):31–37.
21. Connolly RM, Leal JP, Solnes L, et al. Updated results of TBCRC026: phase II trial correlating standardized uptake value with pathological complete response to pertuzumab and trastuzumab in breast cancer. J Clin Oncol 2021;39(20):2247–2256.
22. Groheux D, Mankoff D, Espié M, Hindié E. [18]F-FDG PET/CT in the early prediction of pathological response in aggressive subtypes of breast cancer: review of the literature and recommendations for use in clinical trials. Eur J Nucl Med Mol Imaging 2016;43(5):983–993.
23. Koolen BB, Vogel WV, Vrancken Peeters MJ, Loo CE, Rutgers EJ, Valdés Olmos RA. Molecular imaging in breast cancer: from whole-body PET/CT to dedicated breast PET. J Oncol 2012;2012:438647.
24. Moy L, Ponzo F, Noz ME, et al. Improving specificity of breast MRI using prone PET and fused MRI and PET 3D volume datasets. J Nucl Med 2007;48(4):528–537.
25. Moliner L, Gonzalez AJ, Soriano A, et al. Design and evaluation of the MAMMI dedicated breast PET. Med Phys 2012;39(9):5393–5404.
26. Teixeira SC, Rebolleda JF, Koolen BB, et al. Evaluation of a hanging-breast PET system for primary tumor visualization in patients with stage I-III breast cancer: comparison with standard PET/CT. AJR Am J Roentgenol 2016;206(6):1307–1314.
27. Koolen BB, Vidal-Sicart S, Benlloch Baviera JM, Valdés Olmos RA. Evaluating heterogeneity of primary tumor (18)F-FDG uptake in breast cancer with a dedicated breast PET (MAMMI): a feasibility study based on correlation with PET/CT. Nucl Med Commun 2014;35(5):446–452.
28. Hathi DK, Li W, Seo Y, et al. Evaluation of primary breast cancers using dedicated breast PET and whole-body PET. Sci Rep 2020;10(1):21930.
29. Jafri NF, Newitt DC, Kornak J, Esserman LJ, Joe BN, Hylton NM. Optimized breast MRI functional tumor volume as a biomarker of recurrence-free survival following neoadjuvant chemotherapy. J Magn Reson Imaging 2014;40(2):476–482.
30. Partridge SC, Gibbs JE, Lu Y, et al. MRI measurements of breast tumor volume predict response to neoadjuvant chemotherapy and recurrence-free survival. AJR Am J Roentgenol 2005;184(6):1774–1781.
31. Luporsi E, André F, Spyratos F, et al. Ki-67: level of evidence and methodological considerations for its role in the clinical management of breast cancer: analytical and critical review. Breast Cancer Res Treat 2012;132(3):895–915.
32. Symmans WF, Peintinger F, Hatzis C, et al. Measurement of residual breast cancer burden to predict survival after neoadjuvant chemotherapy. J Clin Oncol 2007;25(28):4414–4422.
33. Hamy AS, Darrigues L, Laas E, et al. Prognostic value of the Residual Cancer Burden index according to breast cancer subtype: validation on a cohort of BC patients treated by neoadjuvant chemotherapy. PLoS One 2020;15(6):e0234191.
34. Campbell JI, Yau C, Krass P, et al. Comparison of residual cancer burden, American Joint Committee on Cancer staging and pathologic complete response in breast cancer after neoadjuvant chemotherapy: results from the I-SPY 1 TRIAL (CALGB 150007/150012; ACRIN 6657). Breast Cancer Res Treat 2017;165(1):181–191.
35. Cho N, Im SA, Cheon GJ, et al. Integrated [18]F-FDG PET/MRI in breast cancer: early prediction of response to neoadjuvant chemotherapy. Eur J Nucl Med Mol Imaging 2018;45(3):328–339.
36. Pengel KE, Koolen BB, Loo CE, et al. Combined use of [18]F-FDG PET/CT and MRI for response monitoring of breast cancer during neoadjuvant chemotherapy. Eur J Nucl Med Mol Imaging 2014;41(8):1515–1524.
37. Goldhirsch A, Winer EP, Coates AS, et al. Personalizing the treatment of women with early breast cancer: highlights of the St Gallen International Expert Consensus on the Primary Therapy of Early Breast Cancer 2013. Ann Oncol 2013;24(9):2206–2223.
38. Mukhtar RA, Yau C, Rosen M, et al. Clinically meaningful tumor reduction rates vary by prechemotherapy MRI phenotype and tumor subtype in the I-SPY 1 TRIAL (CALGB 150007/150012; ACRIN 6657). Ann Surg Oncol 2013;20(12):3823–3830.

39. Price ER, Wong J, Mukhtar R, Hylton N, Esserman LJ. How to use magnetic resonance imaging following neoadjuvant chemotherapy in locally advanced breast cancer. World J Clin Cases 2015;3(7):607–613.
40. Uematsu T, Kasami M, Yuen S. Triple-negative breast cancer: correlation between MR imaging and pathologic findings. Radiology 2009;250(3): 638–647.
41. Chen JH, Agrawal G, Feig B, et al. Triple-negative breast cancer: MRI features in 29 patients. Ann Oncol 2007;18(12):2042–2043.
42. Groheux D, Hatt M, Hindié E, et al. Estrogen receptor-positive/human epidermal growth factor receptor 2-negative breast tumors: early prediction of chemosensitivity with (18)F-fluorodeoxyglucose positron emission tomography/computed tomography during neoadjuvant chemotherapy. Cancer 2013;119(11):1960–1968.
43. Groheux D, Sanna A, Majdoub M, et al. Baseline tumor 18F-FDG uptake and modifications after 2 cycles of neoadjuvant chemotherapy are prognostic of outcome in ER+/HER2- breast cancer. J Nucl Med 2015;56(6):824–831.
44. Hylton NM, Gatsonis CA, Rosen MA, et al. Neoadjuvant chemotherapy for breast cancer: functional tumor volume by MR imaging predicts recurrence-free survival—results from the ACRIN 6657/CALGB 150007 I-SPY 1 TRIAL. Radiology 2016;279(1):44–55.
45. Mema E, Mango VL, Guo X, et al. Does breast MRI background parenchymal enhancement indicate metabolic activity? Qualitative and 3D quantitative computer imaging analysis. J Magn Reson Imaging 2018;47(3):753–759.
46. Leithner D, Baltzer PA, Magometschnigg HF, et al. Quantitative assessment of breast parenchymal uptake on 18F-FDG PET/CT: correlation with age, background parenchymal enhancement, and amount of fibroglandular tissue on MRI. J Nucl Med 2016;57(10):1518–1522.
47. Koo HR, Moon WK, Chun IK, et al. Background ^{18}F-FDG uptake in positron emission mammography (PEM): correlation with mammographic density and background parenchymal enhancement in breast MRI. Eur J Radiol 2013;82(10):1738–1742.
48. Tseng J, Dunnwald LK, Schubert EK, et al. 18F-FDG kinetics in locally advanced breast cancer: correlation with tumor blood flow and changes in response to neoadjuvant chemotherapy. J Nucl Med 2004;45(11):1829–1837.